

RESEARCH ARTICLE

# Simulation of Solid Electrolyte Interphase Growth for Lithium Batteries Based on Kinetic Monte Carlo

Junfu Li\*, Xueli Hu, and Tongxin Li

School of Automotive Engineering, Harbin Institute of Technology, Weihai 264209, Shandong, China.

\*Address correspondence to: [lijunfu@hit.edu.cn](mailto:lijunfu@hit.edu.cn)

Lithium-ion batteries (LIBs) serve as the primary energy source for electric vehicles and smart devices. However, during the usage, the formation of the solid electrolyte interphase (SEI) film is closely related to the capacity decline of the battery, playing a crucial role in the battery performance and lifespan. This study focuses on the growth mechanism of SEI, revealing its evolution during the cycling process of charge and discharge, as well as its impact on the battery's capacity retention and cycle stability. By establishing a simulation model based on the kinetic Monte Carlo (KMC) dynamics method, the dynamic growth process of the SEI on microsecond timescale under various discharge rates is simulated, achieving a quantitative prediction of SEI growth trends. The experimental part uses 18650 LIBs and validates the accuracy of the KMC model through constant current charge–discharge cycle aging experiments, with the simulation error within 4%. The results indicate that the growth rate of the SEI layer gradually increases during charging and decreases during discharging, with more SEI formed during charging than discharging at the same rate. As the number of aging cycles increases, the proportion of capacity loss caused by the SEI first decreases, then increases, and finally decreases again. This finding provides a new perspective for understanding the growth mechanism of the SEI.

## Introduction

In the strategic context of the global energy transition and the pursuit of sustainable development, lithium-ion batteries (LIBs) have emerged as indispensable energy storage elements in electric vehicles, smart devices, and a variety of electronic products due to their exceptional high energy density, prolonged cycle life, and minimal memory effect [1–3]. However, as the operational lifespan of these batteries extends, electrochemical aging becomes increasingly inevitable. The primary aging mechanisms include loss of lithium inventory [4,5], loss of active material [6,7], and loss of electrolyte [8,9], which adversely impact the battery capacity retention, energy efficiency, and cycling stability while simultaneously bringing potential risks of safety and reliability to LIBs [10,11]. The development and thorough investigation of LIB aging models are of paramount importance, which are crucial for elucidating the underlying aging mechanisms, refining battery structural designs, and extending the operational lifespan of batteries, thereby offering important academic and practical benefits.

The solid electrolyte interphase (SEI) plays an important role in the electrochemical aging process of LIBs [12]. On the surface of the graphite anode in LIBs, continuous low-level surface reactions occur between the graphite and the electrolyte, leading to a gradual decrease in recyclable lithium and an increase in electrode impedance during cycling [13,14]. In recent years, numerous studies have endeavored to elucidate the compositional and structural information of the SEI. These extensive investigations

have provided a broad understanding of SEI formation. Peled [15] was the first to introduce the concept of the SEI in 1979, characterizing the electrochemical behavior of alkali and alkaline earth metals in non-aqueous battery systems. Subsequently, in 1983, Aurbach [16] advanced the SEI theory by proposing a dual-layer structural model, which consisted of a thin and dense layer adjacent to the electrode surface and a thicker, porous layer near the electrolyte side. This dual-layer model has deepened the understanding of the complex interplay between the electrode and the electrolyte. Wang et al. [17] employed x-ray tomography imaging to achieve the observation of SEI growth behavior during the lithiation process of batteries, which provided technical support for understanding the complex hierarchical structural features of SEI. Subsequently, Feng et al. [18] further innovated and developed a reflection interference microscopy system that operates under dynamic and nondestructive working conditions, equipped with the capability to real-time imaging during the formation and evolution stages of SEI. This tool reveals the multilayered nature of the SEI structure, specifically the formation of the permanently existing inorganic layer in the interior, the assembly process of the fine structure at the bilayer interface, and the construction of the organic-rich outer layer. A series of findings have significantly enhanced the understanding of the mechanism of SEI dynamic evolution. Wang et al. [19] used *in situ* self-assembly to construct organic/inorganic SEI layers with bilayer ordered structure with the help of highly active fluoride ion-containing electrolyte, which can effectively inhibit the formation and growth of lithium dendrites.

The thickness of SEI is a pivotal parameter influencing the ionic transport characteristics and electrode stability within LIBs [20,21]. Typically, the SEI thickness is on the nanometer scale. By employing sophisticated characterization techniques, Malmgren et al. [22] measured the depth of the SEI layer on the anode of full-cell LIBs, revealing a range from 2 to 46 nm. Similarly, Nie et al. [23] conducted a systematic study on the SEI layer thickness of the graphite anode in LIBs with different electrolyte compositions after a complete lithiation cycle. Their findings indicated a considerable variance in SEI thickness, spanning approximately 10 to 50 nm.

The evolution of electrochemical behaviors and physical properties during the aging of LIBs represents an important area of current research, aiming at delineating the long-term effects of SEI growth on cell performance. Yang et al. [24] employed a physical aging model and highlighted that SEI growth during the initial cycling phase led to a reduction in anode porosity, which in turn could trigger lithium plating near the anode separator after a certain number of cycles. Yang et al. [25] investigated the growth of SEI and lithium dendrites under various rates and temperatures using an electrochemical model, revealing that high rates expedited the loss of anode active material, while the SEI growth rate remained largely unaffected. Ramadass et al. [26] conducted a quantitative analysis of capacity fade on Sony 18650 batteries, specifying the total capacity loss and its constituent factors after 800 cycles at room temperature. Subsequently, Safari et al. [27], assuming no lithium consumption in the cathode, further discussed the anode's contribution to capacity loss and developed a multimodal model grounded in physical phenomena to reveal the kinetic mechanisms of SEI growth. In summary, an in-depth analysis of electrochemical aging models can provide a macroscopic perspective on the role of SEI in the degradation of battery performance. Numerous scholars have delved into the microscale exploration of the structure, composition, growth, and evolution of the SEI in LIBs using research methodologies such as molecular dynamics [28–30], density functional theory [31], and computational reaction network (CRN) [32]. Wang et al. [33] have conducted in-depth characterization of SEI compounds employing techniques like Fourier transform infrared spectroscopy, solid-state nuclear magnetic resonance, x-ray diffraction, and single-crystal x-ray analysis. By comparing the spectra of the SEI thin films derived from ethylene carbonate (EC) and dimethyl carbonate with synthesized model compounds, they have shed light on the potential construction of the SEI, which may consist of a lithium methyl carbonate (LMC)-covered layer of lithium ethylene monocarbonate (LEMC) organic material. Spotte-Smith et al. [34] have further explored the formation and evolution of the SEI membrane using quantum chemical calculations and data-driven CRN. With accelerated simulations at elevated temperatures, the hypothesis of the reduction of LEMC to lithium ethylene dicarbonate (LEDC) and  $H_2$  was corroborated. However, achieving a comprehensive understanding of the exact structure, composition, and functional mechanisms of the SEI membrane remains a challenge in current research.

The kinetic Monte Carlo (KMC) method is widely recognized for its computational efficiency in simulating the dynamical behavior of physical systems, making it particularly well suited for investigating the aging models of LIBs across longer timescales. This approach can capture the dynamic performance variations inherent in the battery aging process. Spotte-Smith et al. [34] directly model the competition between SEI products at the

mechanism level. They obtained the chemical reaction pathways of SEI during formation from the microscopic level with the help of CRN analysis and ab initio calculation methods. Subsequently, the distribution of solid-state products and the average fraction of gaseous by-products during these reactions were quantified using the KMC method. Shinagawa et al. [35] successfully simulated the capacity fade induced by SEI growth through a bidirectional coupling strategy integrating single particle model and KMC model. Their simulation explored the impact of varying lithium-ion conductivity and surface defect constants on the formation rate of SEI. By utilizing the KMC method, Liu et al. [36] constructed a kinetic model for the growth of lithium dendrites, uncovering the intrinsic linkage between the growth characteristics of lithium dendrites and charging conditions. The KMC method has emerged as a novel investigative tool that facilitates a more profound comprehension of the kinetic mechanisms underlying SEI formation and lithium dendrite growth during the aging of LIBs.

To elucidate the morphological changes and heterogeneity of the SEI growth throughout the extended service life of LIBs, and to investigate the phenomena of capacity fade and impedance increase caused by SEI growth, this study employs the KMC method to construct a model of SEI growth throughout the entire life cycle of LIBs. Building on this foundation, the dynamic growth process of the SEI is simulated to deeply explore the growth patterns and morphological evolution during various charge–discharge cycles. The originality of this paper lies in the following: Based on the profound understanding of SEI growth mechanism, a KMC model that can simulate the growth of the SEI on microsecond timescale is developed with the combination of a failure physics model. This model quantifies the capacity fade and impedance increase throughout the entire battery life cycle, both of which are attributed to the evolution of the SEI. The study delves into the growth rates of the SEI during different aging stages under varying charge–discharge rates. The morphology of the SEI at different aging stages has been presented, achieving visualization of the SEI growth process. This provides researchers with an intuitive visual reference. Based on the KMC model, the growth trend of the SEI can be predicted, providing a scientific basis for the safe use and performance optimization of batteries. This research not only offers a new perspective for an in-depth understanding of the SEI growth mechanism but also provides strong support for the future performance enhancement and life extension of LIBs.

The remainder of this work is organized as follows: Materials and Methods first presents the computational method for the SEI based on an electrochemical model, then elaborates on the theoretical framework of this method, including the SEI growth simulation algorithm constructed based on the KMC model, and finally discusses its mathematical principles and implementation details. Experiment is the experimental section, which describes the experimental conditions, subjects, and used equipment. Results and Discussion provides a detailed analysis of the experimental results. Conclusion summarizes the main findings and research sections of this work.

## Materials and Methods

### Electrochemical mechanism-based side reaction model for SEI

The formation of the SEI occurs on the surface of the anode during the initial charge–discharge cycles [34]. SEI film has

lithium-ion conductivity and electronic insulation, which can suppress the continuous decomposition of the electrolyte in subsequent cycles, thereby offering kinetic protection to the anode. The anode materials in LIBs are typically carbon-based, such as graphite or amorphous carbon with high specific surface area and porosity, which can provide numerous reactive sites that facilitate the formation and growth of the SEI on the anode surface.

The growth of the SEI consumes active lithium ions, leading to an irreversible reduction in cell capacity. The total lithium content  $Q_{Li}$  can be calculated based on the capacities of the anode and cathode, as well as their initial lithium intercalation levels [37]. The simplified electrochemical (SP+) model and the parameters used for characteristic simulation in this work are presented in the Supplementary Materials. The definition of  $Q_{Li}$  is given as

$$Q_{Li} = Q_n x_0 + Q_p y_0 \quad (1)$$

where  $Q_p, Q_n$  is the capacity of the cathode and anode electrode and  $x_0, y_0$  is the initial lithium intercalation amount in the anode and cathode.

In SP+ model, the calculation of the reaction polarization overpotential at the anode boundary is presented as follows [38]:

$$\eta_n = \frac{2RT}{F} \cdot \ln \left( \sqrt{m_n^2 + 1} + m_n \right) \quad (2)$$

$$m_n = \frac{0.5}{3Q_n(c_0 + \Delta c)^{0.5}} \frac{1}{\left(1 - x_{surf}\right)^{0.5} \left(x_{surf}\right)^{0.5}} P_{act\_n} \cdot I \quad (3)$$

$\eta_{SEI}$  is the local overpotential of the SEI with the expression detailed as follows [25]:

$$\eta_{SEI} = U_n + \eta_n - U_{SEI}^{ref} \quad (4)$$

where  $U_n$  is the solid-phase open-circuit potential at the anode current collector boundary,  $\eta_n$  is the reaction polarization overpotential at the anode boundary, and  $U_{SEI}^{ref}$  is the local equilibrium potential associated with the formation of the SEI [39]. As the battery undergoes cycling, the chemical composition and structure of the SEI become relatively stable. Tafel equation that describes the rate of the SEI side reactions is used to calculate the relationship between side reaction overpotential and reaction ion current density  $j_{SEI}$  [26]

$$j_{SEI} = -a_n i_{SEI} \exp \left( -\frac{\alpha_s F}{RT} \eta_{SEI} \right) \quad (5)$$

where  $a_n$  is the specific surface area of the anode,  $i_{SEI}$  is the exchange current density of SEI,  $\alpha_s$  is the exchange coefficient of the SEI,  $F$  is the Faraday constant,  $R$  is the universal gas constant, and  $T$  is the temperature.

In accordance with the law of mass conservation, the rate of growth of the SEI at various locations on the anode of LIBs is as follows:

$$\frac{\partial \delta_{SEI}}{\partial t} = -\frac{M_{SEI} j_{SEI}}{a_n \rho_{SEI} F} \quad (6)$$

where  $M_{SEI}$  is the average molar mass of the SEI and  $\rho_{SEI}$  is the average density of the SEI. The distribution of SEI internal resistance in this work is given by:

$$R_{SEI}(t) = R_{SEI} + \frac{\delta_{SEI}(t)}{\kappa_{SEI}} \quad (7)$$

where  $\kappa_{SEI}$  is the electrical conductivity of the SEI. The relationship between the battery capacity  $Q_{SEI}$  consumed by SEI side reactions and  $j_{SEI}$  is expressed as follows:

$$\frac{\partial Q_{SEI}}{\partial t} = A \delta_n j_{SEI}(t) \quad (8)$$

where  $\delta_n$  represents the thickness of the anode current collector.

## Simulation of SEI growth based on the KMC model

Although atomic/molecular simulations at the microscopic scale are precise, they are limited by the scales of time and space, making it difficult to encompass the entire lifespan of a battery. To address this problem, the KMC method has been adopted. This method simulates the stochastic transitions of system states, effectively extending the timescale to cover durations from microsecond to much longer periods while retaining key kinetic characteristics and improving computational efficiency. The KMC method not only overcomes the limitations of traditional simulations but also provides a new perspective for deeply understanding the SEI growth mechanism and its impact on battery performance. It holds significant importance for the optimization of battery design and the prediction of service life. In this part, a KMC model of SEI is constructed to simulate the growth process of the SEI, quantifying its capacity and impedance.

## Composition and structure of SEI

The structure and components of SEI are complex, and its dynamic characteristics run through the whole life cycle of the battery. The SEI is primarily composed of inorganic inner layer and organic outer layer, exhibiting high heterogeneity in its growth process. Adjacent to the anode surface, it includes dense inorganic compounds such as lithium carbonate ( $\text{Li}_2\text{CO}_3$ ), lithium oxide ( $\text{Li}_2\text{O}$ ), and lithium fluoride ( $\text{LiF}$ ) on the graphite side, with  $\text{Li}_2\text{CO}_3$  being the first component of the inner layer. On the electrolyte side, loosely bound organic materials are present, such as alkyl carbonates and polymers.

With electrolyte composed of lithium hexafluorophosphate ( $\text{LiPF}_6$ ) and EC, the initial reduction reaction of the electrolyte is mainly driven by the reduction of EC. As the potential of the negative electrode decreases, EC decomposes on the surface of the negative electrode, producing a film dominated by LEDC and LiF, with  $\text{C}_2\text{H}_4$  being the main gaseous by-product. LEMC and inorganic carbonates are important minority components. When the electrode potential is reduced to the reduction potential of  $\text{Li}^+/\text{EC}$ , EC, along with LEDC and LEMC, is reduced to form inorganic carbonates that deposit on the electrode surface, releasing  $\text{C}_2\text{H}_4$  and CO. After the initial layer is formed, the SEI continues to grow outward over time. Lithium carbonate salts, such as LEDC, LEC, and LMC, undergo a continuous decomposition to produce a variety of products such as  $\text{Li}_2\text{CO}_3$ , lithium alcohol, LiF, and  $\text{CO}_2$ . The precipitation of these products causes the SEI to become loose and porous, leading to electrolyte infiltration. The SEI continues to undergo decomposition reactions, forming a cyclic mechanism of continuous thickening and compositional remodeling of the SEI. During this

process, the inorganic region of the SEI grows with the decomposition of LEDC to form inorganic carbonates and  $C_2H_4$  [27,34], where  $Li_2CO_3$  is the first component of the inner layer.

This study focuses on the effect of SEI on battery performance. The continuous accumulation and reconfiguration of  $Li_2CO_3$  leads to irreversible depletion of active lithium ions, which directly reduces the effective capacity of the battery and has been shown to be one of the main drivers of battery capacity degradation. In the model, the SEIs are assumed to be  $Li_2CO_3$  crystals, which have been extensively studied, preserving the central role of SEI in the evolution of battery performance.

To model the growth of the SEI with the KMC method, the structure of  $Li_2CO_3$  has been simplified. Assuming that the SEI is composed of a crystalline phase  $Li_2CO_3$ , the crystal lattice structure of  $Li_2CO_3$  exhibits typical monoclinic symmetry, with unit cell parameters of  $a = 8.359\text{ \AA}$ ,  $b = 4.973\text{ \AA}$ , and  $c = 6.197\text{ \AA}$  and cell angles  $\alpha = 90.00^\circ$ ,  $\beta = 114.83^\circ$ , and  $\gamma = 90.00^\circ$  [40]. The unit cell is simplified to a body-centered tetragonal structure, with the base area of the unit cell  $s_0$  being:

$$s_0 = \frac{a \times b}{2} = 2.0785 \times 10^{-19}\text{ m}^2 \quad (9)$$

The height of the unit cell is given by:

$$h = \frac{c \sin\beta}{2} = 2.8121 \times 10^{-10}\text{ m} \quad (10)$$

## Establishment of spatial dimensions in the KMC model

The KMC model is focused on the surface of the anode current collector. The measured thickness of the SEI on the graphite anode varies, ranging from approximately 10 to 50 nm, significantly smaller than the radius of the anode active particles. Consequently, it is considered that the SEI grows on the surface of the current collector, expanding outward perpendicularly to the surface. Considering that there is no significant correlation between grid size and simulation accuracy, a grid system of  $x \times y \times z = 50 \times 50 \times \infty$  is considered, with each grid unit's area equivalent to the base area of crystal cell  $Li_2CO_3$ .

The initially established grid structure was refined. The SEI in the fresh cell exhibits a resistance of  $0.001\text{ \Omega m}^2$  [41], with a thickness of 5 nm according to the ionic conductivity of  $Li_2CO_3$ . Given the height of  $Li_2CO_3$  unit cell as per Eq. 7, it is assumed that each grid cell initially contains 18 such unit cells. During the subsequent simulation, only the formation of  $Li_2CO_3$  unit cells is considered with the neglect of their interactions. In this approach, it is assumed that each unit cell can only occupy one grid cell and will not vanish upon formation.

## KMC-based model for SEI growth

The multi-scale model employed in this study is established by integrating the SP+ model for SEI growth with the KMC model [35], as depicted in Fig. 1, which illustrates the flowchart of a

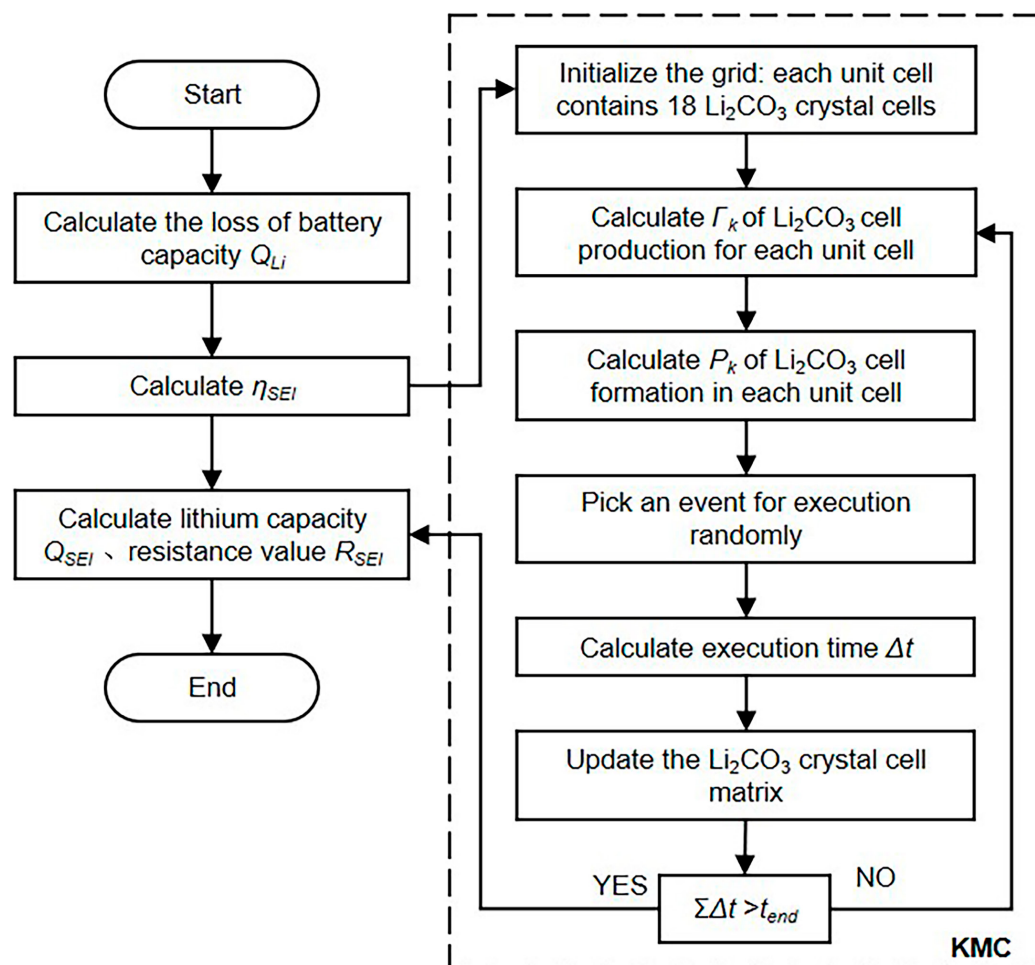


**Fig. 1.** Schematic of the KMC-based SEI growth model simulation process.

single charge-discharge cycle simulation within the multi-scale model framework.

Step 1: Calculate the growth rate of  $\text{Li}_2\text{CO}_3$  unit cells in each grid cell at any given moment, and sum these rates to obtain cumulative growth rate of the model. Divide the growth rate of  $\text{Li}_2\text{CO}_3$  unit cells in each grid cell by the model's cumulative growth rate to determine the occurrence probability of  $\text{Li}_2\text{CO}_3$  unit cells in each grid cell. By modifying the Tafel equation, the formation rate of the SEI can be expressed as:

$$\Gamma = K \exp\left(-\frac{F}{2RT}\eta_{SEI}\right) \quad (11)$$

where  $K$  is the reaction rate constant of SEI. The expression for the SEI reaction rate constant  $K$  is as follows:

$$K = \frac{i_{SEI} s_0 N_A J_{SEI}}{2F} \quad (12)$$

where  $s_0$  is the base area of the unit cell,  $N_A$  is Avogadro's constant, and  $J_{SEI}$  is the reaction rate coefficient of the SEI.

The inhomogeneity of the surface topography of the negative electrode contributes to the formation process of the SEI by affecting several aspects, such as electrolyte distribution, reactivity, local electrochemical reaction environment, and mechanical stress, leading to differences in its thickness and properties in different regions. The formation rate of  $\text{Li}_2\text{CO}_3$  cells at surface defects is thus greater than that on the terraces. Therefore, if at least one adjacent unit cell within the same layer is occupied, the formation rate of  $\text{Li}_2\text{CO}_3$  unit cells in that unit cell is given by the following expression:

$$\Gamma = QK \exp\left(-\frac{F}{2RT}\eta_{SEI}\right) \quad (13)$$

where  $Q$  is a constant related to electrochemical properties.

Calculate the formation rate  $\Gamma_k$  of  $\text{Li}_2\text{CO}_3$  unit cells at the vacancy sites on the lowest layer of each grid cell, as depicted in Fig. 2B, where  $k$  ( $k = 1, 2, 3, \dots, N$ ) is the identifier for each grid cell and  $N$  is the total number of grid cells. A "null event" refers to an occurrence that does not form  $\text{Li}_2\text{CO}_3$  cells, characterized by a constant rate of occurrence and a relatively small value. Without considering the introduction of "null event", the

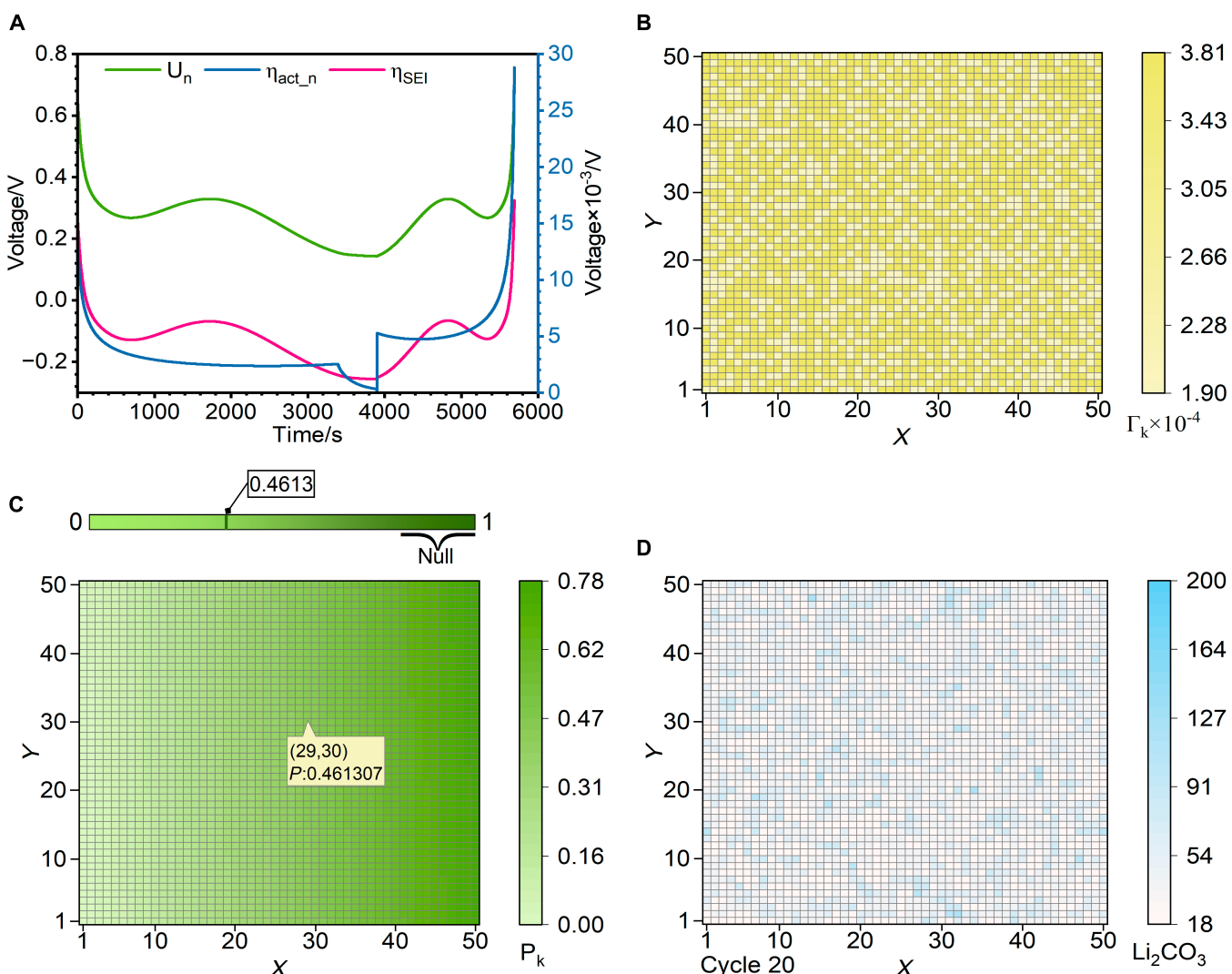


**Fig. 2.** Schematic of key steps in KMC-based SEI growth simulation. Illustrated with the 20th aging cycle, (A) calculation of  $\eta_{SEI}$ . (B and C) Computation and determination of the probability of  $\text{Li}_2\text{CO}_3$  unit cell formation rates for each grid cell. (D)  $\text{Li}_2\text{CO}_3$  unit cell matrix after 20 aging cycles.

**Table.** The value of parameters used in KMC model

Parameter	Definition	Value
$U_{SEI}^{ref}(V)$	Local equilibrium potential for SEI formation	0.4
$j_{SEI}(A m^{-3})$	Side reaction rate of SEI film	-
$a_n(m^{-1})$	Specific surface area	240,000
$i_{SEI}(A m^{-2})$	Exchange current density of SEI film	-
$\alpha_s(-)$	Transfer coefficient	0.5
$F(C mol^{-1})$	Faraday's constant	96,587
$R(J mol^{-1} K^{-1})$	Universal gas constant	8.314
$M_{SEI}(kg mol^{-1})$	Average molar mass of the SEI film	0.165
$\rho_{SEI}(kg m^{-3})$	Average density of the SEI film	1,600
$\kappa_{SEI}(s m^{-1})$	Conductivity of the SEI film	$5 \times 10^{-6}$
$\delta_n(m)$	Thickness of electrode	$10^{-4}$
$s_0(m^2)$	Crystal cell base area	$2.0785 \times 10^{-19}$
$h(m)$	Crystal cell height	$2.8121 \times 10^{-10}$
$N_A(mol^{-1})$	Avogadro constant	$6.02 \times 10^{23}$
$Q(-)$	A constant related to surface defects	2
$\Gamma_{null}(s^{-1})$	The occurrence rate of "null event"	0.05625
$A(m^2)$	Surface area	0.1
$S(m^2)$	Total grid area	$5.1962 \times 10^{-16}$

calculated capacity decay and impedance of the SEI will be greatly increased. In addition, the calculation time of the KMC model will also increase. Therefore, the "null event" is considered as the  $(N + 1)$ th event.

Step2: Store the rates of  $Li_2CO_3$  unit cell formation for all grid cells and the occurrence rates of "null events" in a matrix  $\Gamma_{N+1}$ , and define  $\Gamma'_k = \sum_{j=1}^k \Gamma_j$ , where  $k = 1, 2, 3, \dots, N, N + 1$ . Calculate the probability  $P_k$  of the  $k$ th event occurring:

$$P_k = \frac{\Gamma_k}{\sum_{k=1}^{N+1} \Gamma_k} \quad (14)$$

$$\Gamma = [P_1, P_2, P_3, \dots, P_N, P_{N+1}] \quad (15)$$

Step3: Generate a random number  $\xi_1 \in (0,1)$  and identify the probability range within which one of the  $N + 1$  events occur, such as  $\Gamma'_{k-1} \leq \xi_1 \leq \Gamma'_k$  ( $k = 1, 2, 3, 4, \dots, N, N + 1$ ) Based on this random number, select and execute the  $k$ th event, as illustrated in Fig. 2C.

Step4: Generate an additional random number  $\xi_2 \in (0,1)$ , calculate the time step required to execute the  $k$ th event, and update the distribution matrix of the  $Li_2CO_3$  unit cells, as depicted in Fig. 2D. The expression for the time step  $\Delta t_{SEI}$  is presented as follows:

$$\Delta t_{SEI} = -\frac{\ln \xi_2}{\sum_{k=1}^{N+1} \Gamma_k} \quad (16)$$

The simulation model is terminated when the sum of the time steps in the KMC model equals the discharge duration of an aging experiment.

At any given moment, the number of  $Li_2CO_3$  unit cells generated within the grid cells through KMC model simulation is  $H_k$ , and the average number of  $Li_2CO_3$  unit cells across the grid is:

$$H_{ave} = \frac{\sum_{k=1}^N H_k}{N} \quad (17)$$

The average thickness of the SEI on the surface of the anode current collector is given by:

$$\delta_{ave} = H_{ave} h \quad (18)$$

where  $h$  is the height of the  $Li_2CO_3$  unit cell.

The ohmic internal resistance of the SEI is expressed as:

$$\Delta R_{SEI} = \frac{\delta_{ave}}{\kappa_{SEI}} \quad (19)$$

Additionally, since each  $Li_2CO_3$  unit cell contains 8 units of  $Li^+$ , the amount of  $Li^+$  charge within the SEI formed on the surface of the anode current collector through KMC model simulation is given by:

$$\Delta Q_{SEI} = 8H_{ave} \frac{A}{S} \frac{F}{N_A} \quad (20)$$

where  $H_{ave}$  is the total number of  $Li_2CO_3$  unit cells within the grid,  $A$  is the surface area of the anode current collector, and  $S$  is the total area of the grid. Simulations were conducted using the KMC model, with the parameters listed in Table.

## Experiment

To acquire insights into the growth of the SEI under various aging conditions and to validate the precision of the KMC

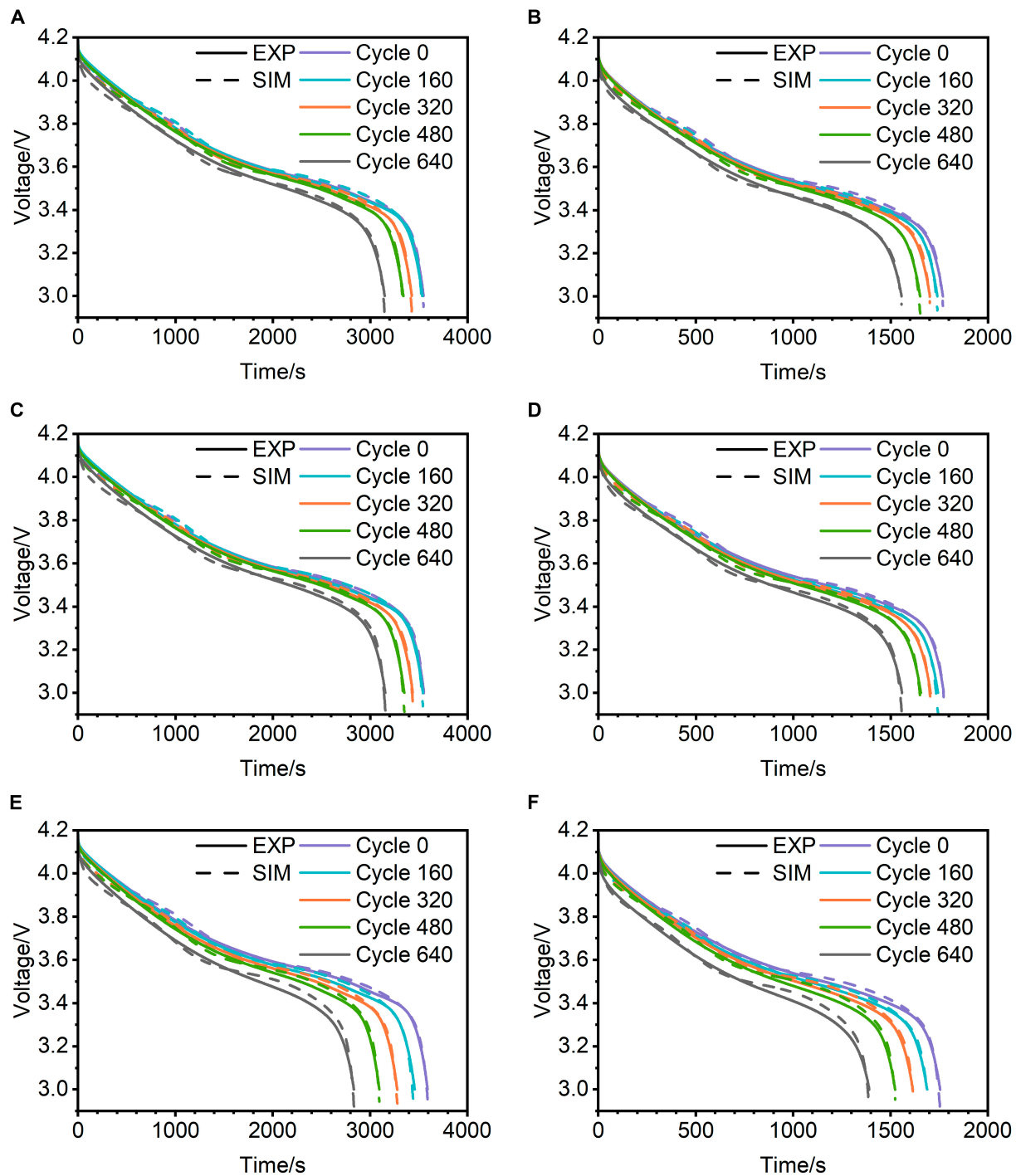


**Fig. 3.** Simulated terminal voltage results of (A and B) Cell No. 1, (C and D) Cell No. 2, and (E and F) Cell No. 3. under various conditions.

model, a series of aging experiments were designed under multiple operational conditions.

To validate the applicability of the simulation model, aging experiments were carried out on 18650 LIBs with a capacity of 2 Ah. During the charge and discharge processes, the terminal voltage and current data of the batteries were collected using the BTS-5V-20A charge-discharge testing instrument from Shenzhen Neware Company, with the battery environment controlled by a constant temperature chamber.

Battery aging is influenced by a variety of external factors, such as temperature, humidity, charge-discharge rates, and

depth of discharge, each of which has a distinct impact on the aging mechanisms of the battery. To prevent the side reaction of lithium plating, the experiment was conducted at a constant temperature of 25°C, considering only the impact of charge-discharge rates on battery aging. A total of 3 sets of experiments were conducted, including constant current charge-discharge cycle aging experiments, parameter identification experiments, and performance testing experiments, with the voltage range spanning from full charge to full discharge.

The cycle aging experiments used a method of constant current-constant voltage charging and constant current

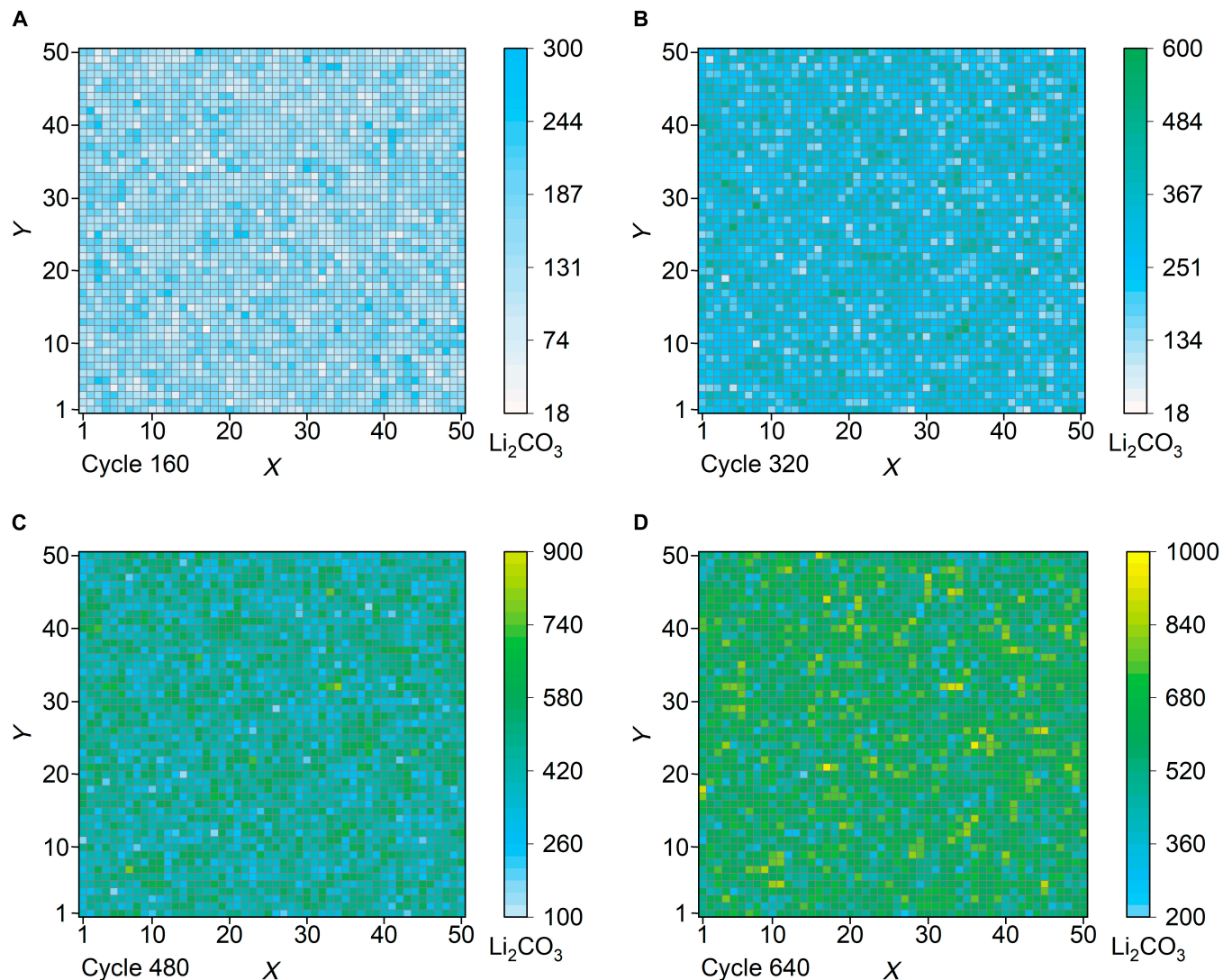


**Fig. 4.** SEI growth of Cell No. 1 at cycle 160 (A), 320 (B), 480 (C), and 640 (D) aging cycles.

discharging. Initially, the battery was charged in constant current at 1 C rate. When the battery voltage reached 4.2 V, the charging current was gradually reduced to maintain the voltage at 4.2 V until the charging current was less than 0.05 C. After the battery was left to rest for 15 min, it was discharged at a rate of 2 C until the voltage drops to the cutoff voltage, at which point the discharge was stopped. After another 15 min of rest, the next aging cycle began. The parameter identification experiment involved performing a short-term constant current discharge at a rate of 0.5 C on the battery, and the battery capacity measured under this condition was used as the standard capacity to calculate the battery state of health. The performance testing experiment involved conducting 1 C and 2 C constant current discharge test on the battery every 40 cycles during the charge-discharge cycle process.

The parameters identified from the SP+ model at various aging cycles were incorporated into the SEI side reaction model. The terminal voltage curves of the battery under 1 C and 2 C constant current discharge conditions were fitted and compared with the actual terminal voltage curves to verify the accuracy of the SEI side reaction model. The simulation results of the terminal voltage fitting and actual

measured curves under different conditions and cycle numbers are shown in Fig. 3.

Upon examining the terminal voltage measured curves and simulated curves at various discharge rates and aging stages, it is observed that the electrochemical model incorporating the SEI demonstrates a good fit throughout the early, middle, and late stages of battery aging. There is no significant decrease in the simulation accuracy of the external characteristics with the increase in the degree of aging. The average errors between the fitted terminal voltage curves and the measured curves for 1 C and 2 C constant current discharge are 15.73 and 17.4 mV, respectively. The SEI electrochemical model maintains a high degree of consistency across different discharge rates and aging cycles.

The electrochemical model can calculate key parameters such as the thickness, impedance, and capacity loss of the SEI. The KMC method simulates the growth process of the SEI formation by modeling the random motion of microscopic particles, thereby predicting its morphological changes, impedance increase, and capacity decay. To verify the accuracy of the KMC model's simulations, this study compares the results of SEI thickness, impedance, and capacity loss obtained from the

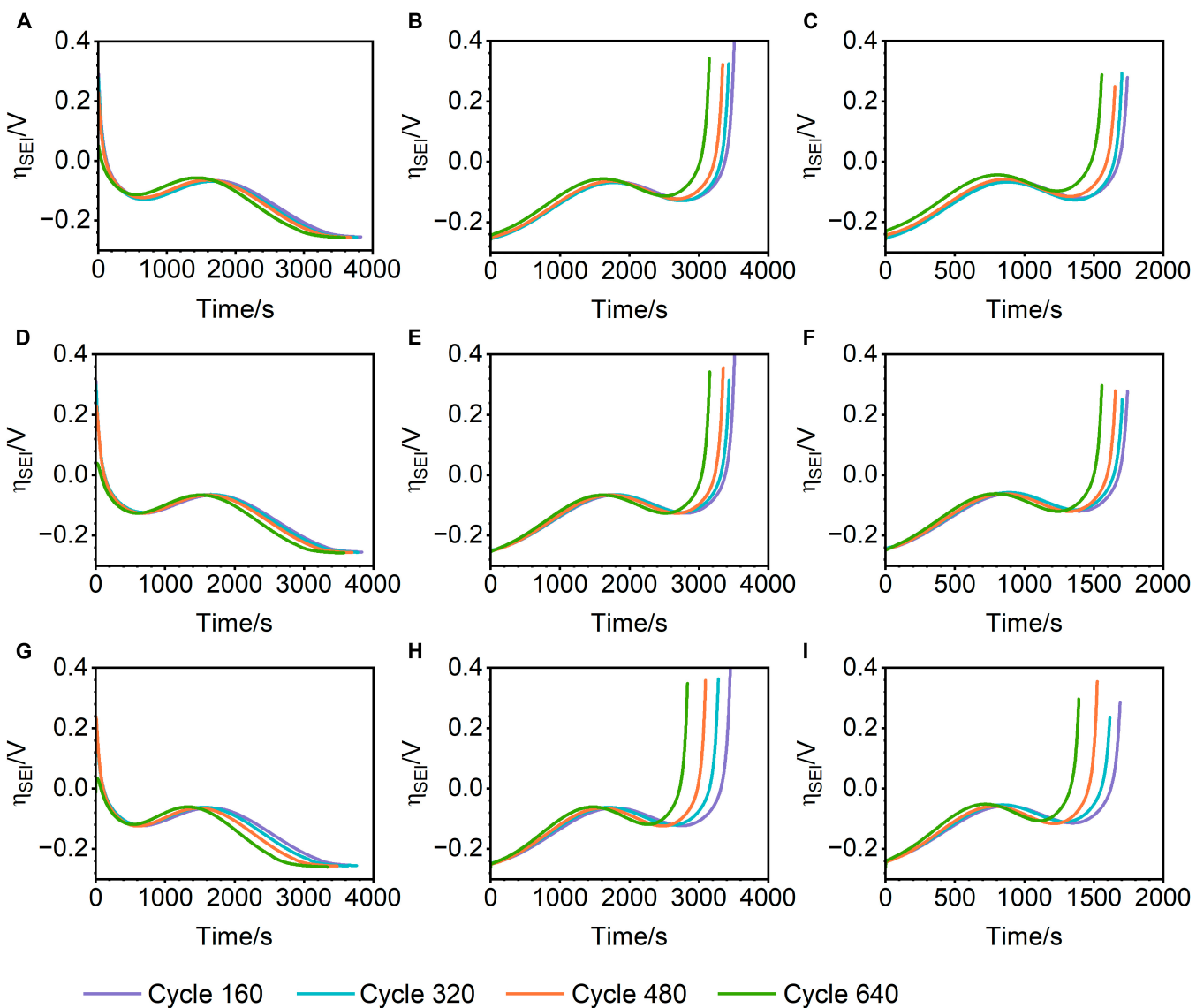


**Fig. 5.** The local overpotential of SEI at (A to C) Cell No. 1, (D to F) Cell No. 2, and (G to I) Cell No. 3 at 1 C charge, 1 C discharge, and 2 C discharge across varying aging cycles.

electrochemical model with those derived from the KMC model simulations. A cross-validation approach is employed to ensure the reliability and accuracy of the results.

## Results and Discussion

Based on the cyclic aging experiments established, the growth process of the SEI over different aging cycles was simulated. Figure 4 illustrates the growth of the SEI on the surface of the anode current collector of Cell No. 1 under constant current charge at 1 C and constant current discharge at 2 C across different aging cycles. Figure 4 represent the SEI growth states after 160, 320, 480, and 640 aging cycles, showing an increase in SEI thickness and coverage with the extension of the aging cycle. In the early stages of battery aging, the unevenness of the electrochemical reactions leads to uneven SEI growth. As the number of cycles increases, the SEI coverage on the electrode surface becomes more uniform. Meanwhile, the heterogeneity in the thickness of SEI layer also becomes increasingly apparent. In addition to considering the unevenness of the electrochemical

reactions, the growth rate at the stepped areas on the SEI surface is significantly higher than that at other locations, further contributing to the unevenness of SEI growth.

Figure 5 illustrates the evolution curves of  $\eta_{SEI}$  at different cycle periods under 1 C charge rate, 1 C discharge rate, and 2 C discharge rate. The results show that during the 1 C charge process, the potential of the battery's anode tends to decrease, leading to a corresponding decrease in  $\eta_{SEI}$ . According to Eq. 11, the formation rate of the unit cell at the vacancy points on the bottom layer of the cell will increase accordingly, causing the growth rate of the SEI to show an upward trend. Therefore, the formation rate of the SEI is relatively slow at the beginning and faster at the later stage during charging, which accelerates the decomposition of the electrolyte on the surface of the anode. In contrast, during the 1 C and 2 C discharge processes, the curve of  $\eta_{SEI}$  generally shows an upward trend and the formation rate of the unit cell at the vacancy points on the bottom layer of the cell will decrease accordingly, leading to a faster formation rate of the SEI at the beginning and a slower rate at the later stage.

Additionally, when charging and discharging at the same rate, the local overpotential of the SEI during charging is generally lower than that during discharging. This results in a greater formation of SEI during the charging process compared to the discharging process.

Figure 6 illustrates the growth of the SEI on the surface of the anode current collector of Cell No. 2 under constant current charge at 1 C and constant current discharge at 2 C across different aging cycles, where Fig. 6A to D represent the state of the SEI after 160, 320, 480, and 640 aging cycles, respectively. Figure 7 illustrates the growth of the SEI on the surface of the anode current collector of Cell No. 3.

Figure 8 presents the simulation results of capacity loss (Fig. 8A and C) and impedance increase (Fig. 8B and D) caused by SEI growth after a single aging cycle, a single charge, and a single discharge of the batteries, based on electrochemical models and the KMC model. For Cell No. 1 after a single aging cycle, the simulated errors due to SEI growth in lithium loss and internal resistance increase are 1.29% and 2.33%, respectively. For Cell No. 2, the corresponding errors are 1.77% and 3.25%, respectively. For Cell No. 3, the simulation errors for lithium loss and internal resistance growth are 1.78% and 2.26%. These

simulation errors are mainly caused by a combination of the simplified treatment of the SEI model, the accuracy of the KMC model parameters, and the randomness of the KMC model simulation results.

At the 1 C charge rate, the capacity loss and impedance increase caused by SEI growth, as well as the observed number of lithium carbonate crystalline cells, are approximately 4 times that observed at the 2 C discharge rate. This phenomenon was attributed to the significantly higher SEI growth rate during 1 C charging compared to 2 C discharging, as well as the simulation time at the 1 C charge rate being slightly more than twice that of the 2 C discharge rate. Over the longer simulation time, the battery undergoes more electrochemical reaction cycles, allowing the SEI more time and conditions to grow and restructure, resulting in the formation of more lithium carbonate crystalline cells and a greater capacity loss and impedance increase.

The average value of the battery capacity decline before and after 40 aging cycles was taken as the loss of capacity  $Q_{Loss}$  for a single aging cycle. Figure 9A and C provides the quantity of lithium carbonate crystal cells increased on the anode surface after every 40 aging cycles. Figure 9B and D, in the form of a compound chart, displays the total capacity loss  $Q_{Loss}$  of the

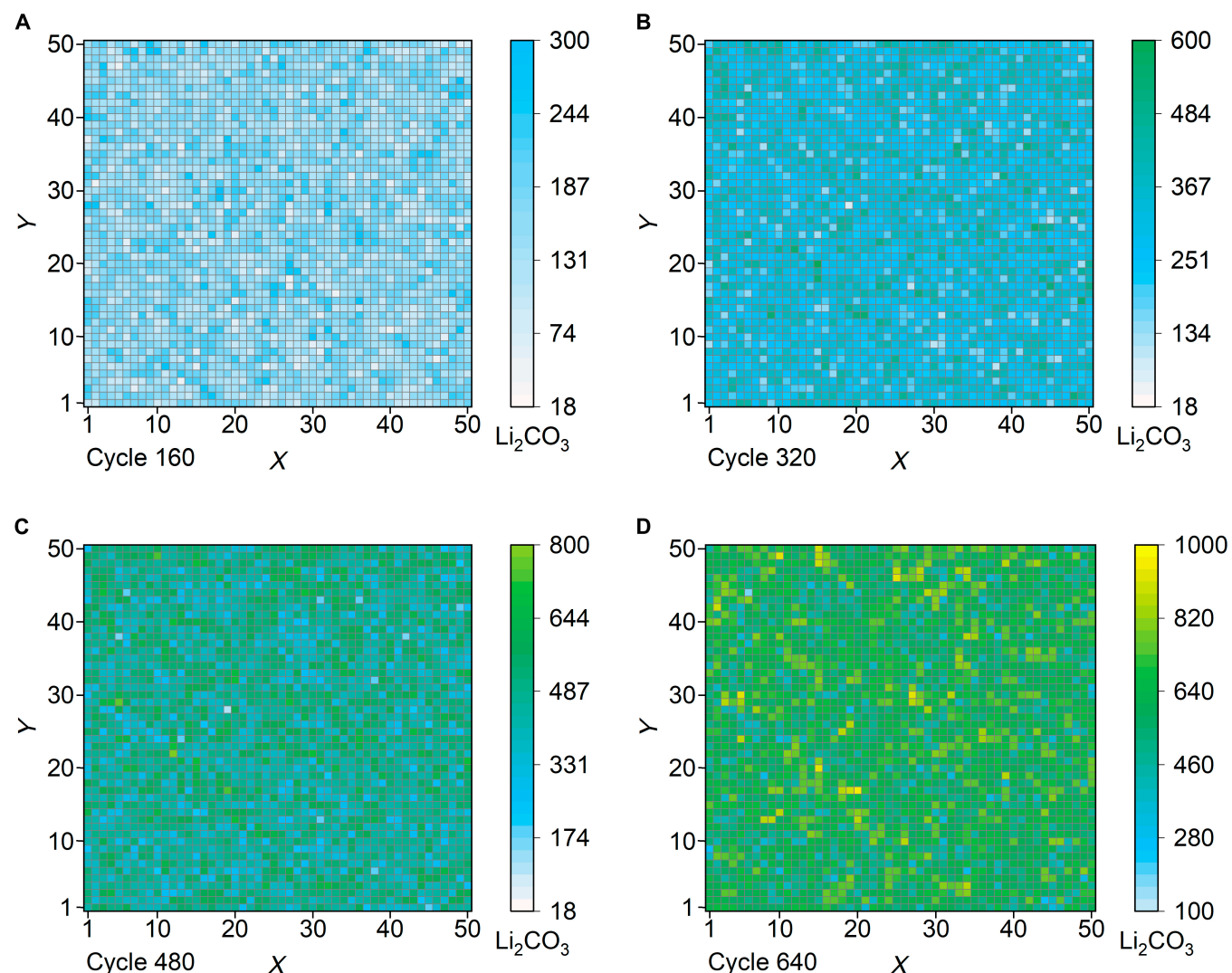
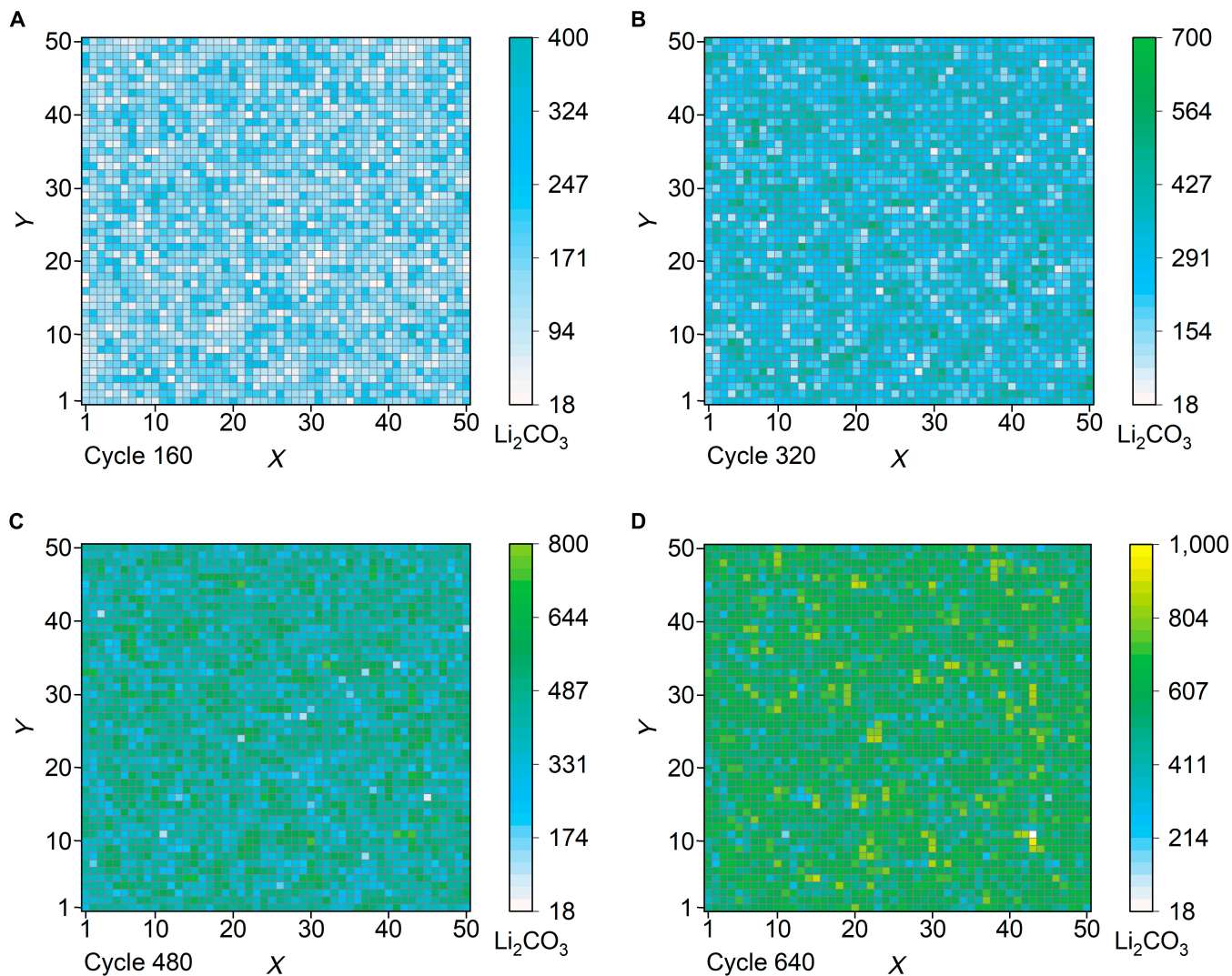


Fig. 6. SEI growth of Cell No. 2 at cycle 160 (A), 320 (B), 480 (C), and 640 (D) aging cycles.



**Fig. 7.** SEI growth of Cell No. 3 at cycle 160 (A), 320 (B), 480 (C), and 640 (D) aging cycles.

battery in a single aging cycle (represented by a bar chart) and the proportion of capacity loss  $Q_{Loss}$  caused by SEI growth to the total capacity loss  $Q_{Loss}$  (represented by a scatterplot). The results show that during the aging cycle process, the proportion of  $Q_{Loss}$  first decreases, then increases, and finally decreases again.

During the first charging and discharging process of the battery, some of the electrolyte components begin to undergo reduction or decomposition reactions on the electrode surface to form the initial nuclei of SEI. After the initial stage of nucleation, SEI begins to enter the 2-dimensional growth stage. A large number of active lithium ions are consumed in the formation of SEI, which rapidly generates a continuous thin-film layer, thus causing a large initial capacity loss.

As the SEI gradually covers the electrode surface, the direct contact area between the electrode and the electrolyte decreases, and the reaction rate of the electrolyte components on the electrode surface decreases. At this stage, the SEI layer continues to grow, but the effect on capacity is relatively reduced. Some of the SEI layers may begin to have some ionic conductivity, which relieves some of the transmission resistance. As a result, the percentage of capacity loss due to SEI is temporarily reduced.

With the charging and discharging cycles, SEI is no longer limited to 2-dimensional growth and begins to undergo expansion and remodeling in the 3-dimensional direction. The SEI layer undergoes further physicochemical changes such as compositional reorganization, structural disruption, and sustained reaction with the electrolyte. These changes are often accompanied by greater consumption of active lithium and irreversible capacity loss. In addition, prolonged cycling may also lead to cracking or peeling in the SEI layer. These defects can further accelerate the decomposition of the electrolyte and the corrosion of the active material, thereby exacerbating capacity degradation. At this stage, the thickness of SEI changes significantly to adapt to the electrochemical environment during battery operation. At this time, the percentage of capacity loss caused by the SEI layer will rise again and become a non-negligible part of the total capacity loss of the battery.

After continuous aging, the SEI gradually becomes dense and stable, forming a protective layer with a certain thickness and structure. The dense SEI layer can more effectively prevent the solvent molecules and dissolved lithium salts in the electrolyte from reacting with the electrode material, thus reducing the further growth of the SEI layer. However, in our experimental design, the cells were aged to a higher degree of 85%,

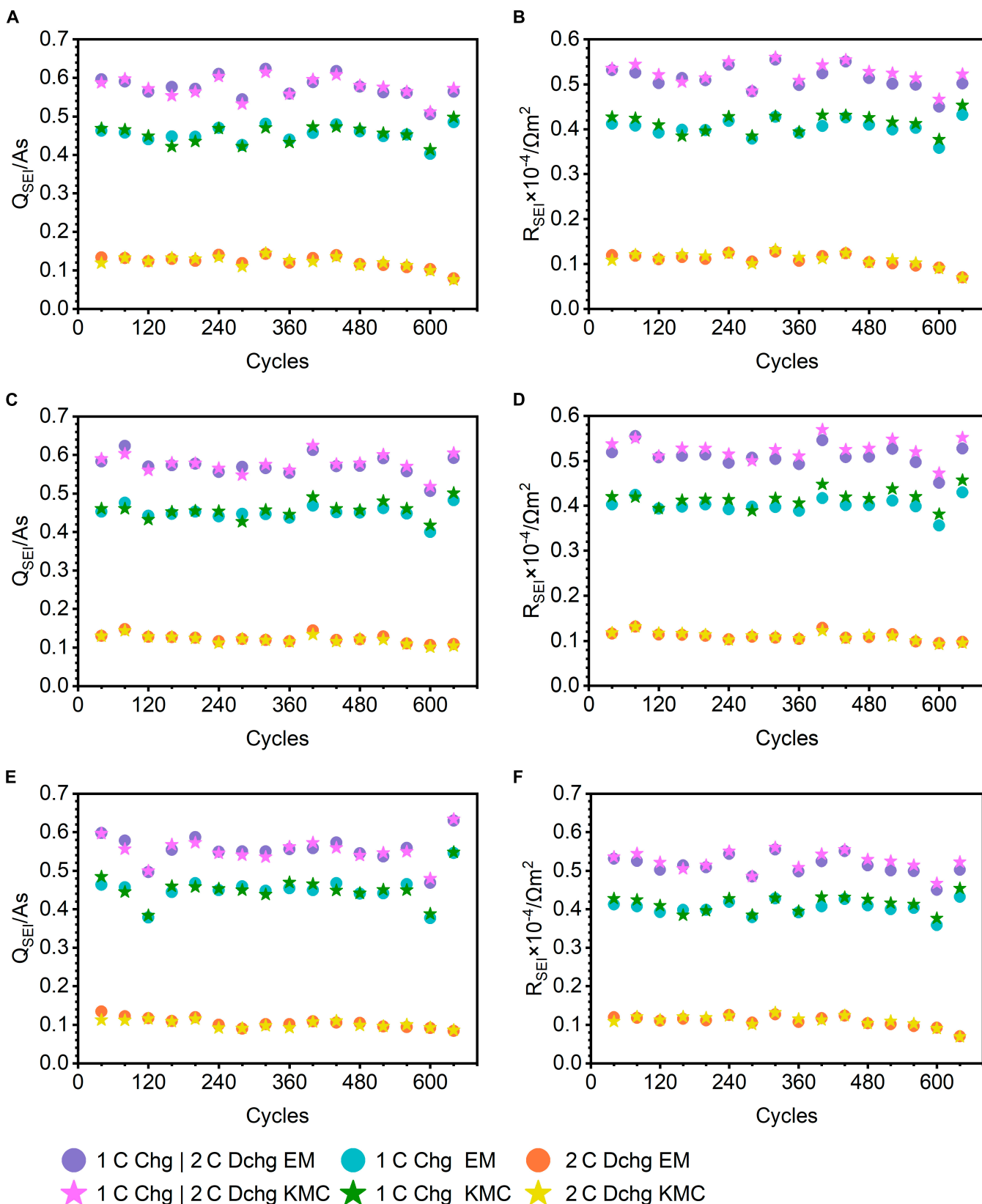


**Fig. 8.** Capacity loss and impedance increase of (A and B) Cell No. 1, (C and D) Cell No. 2, and (E and F) Cell No. 3 due to SEI growth after a single aging cycle.

which did not reach the critical point for decommissioning. This resulted in the SEI layer still being in a relatively active growth phase, failing to fully exhibit the dense and stable state it can achieve at lower aging levels.

In summary, the effect of SEI on the percentage of capacity loss during the aging cycle shows a complex trend of decreasing, then increasing, then decreasing again. This phenomenon is very clear in the result analysis of Cell No. 1 and Cell No. 2. In contrast,

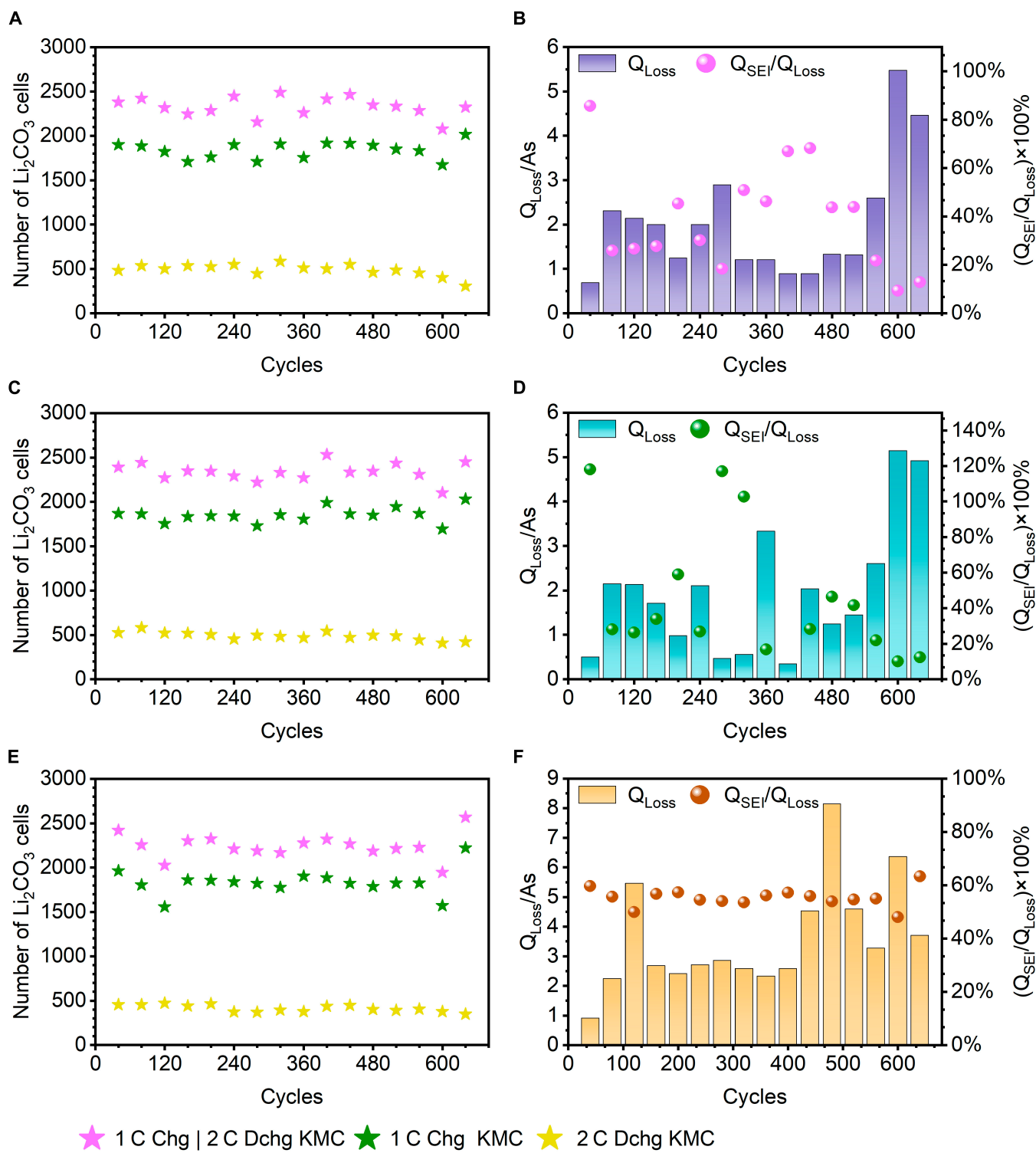


**Fig. 9.** Quantity of lithium carbonate crystal cells formed and proportion of lithium consumption of (A and B) Cell No. 1, (C and D) Cell No. 2, and (E and F) Cell No. 3 by SEI growth after a single aging cycle.

the change in the percentage of capacity loss due to SEI demonstrated by Cell No. 3 is not as significant as the previous 2. This phenomenon is attributed to other more significant capacity loss mechanisms that may be present in Cell No. 3, such as active material detachment, collector corrosion, or internal short circuits. These factors are more dominant in Cell No. 3, thus relatively diminishing the significance of the percentage of capacity

loss in the SEI layer. Nevertheless, it is still recognizable that the percentage of capacity loss of SEI in Cell No. 3 follows the same trend of decreasing, then increasing, then decreasing.

In the analysis of the experimental data for Cell No. 2, a special case arose where the calculated value of the percentage of capacity loss due to SEI exceeded the 100% threshold. This phenomenon stems from the use of a specific calculation

method. The total battery capacity degradation before and after 40 aging cycles is spread evenly over each cycle as an estimate of capacity loss for a single aging cycle. This averaging fails to take into account the variability of SEI's contribution to capacity losses at different cycle stages. As a result, in some scenarios, the estimated value of the SEI's capacity loss share appears to be outside the realm of actual physical significance.

## Conclusion

In the performance and lifespan assessment of lithium batteries, the growth of the SEI plays a crucial role. This study assumed that the SEI was composed of  $\text{Li}_2\text{CO}_3$  unit cells and had constructed a growth model of the SEI based on the KMC method. The model simulated the growth pattern of the SEI throughout the entire life cycle of the lithium battery under normal temperature, providing a quantitative description of the capacity decay and impedance increase that were caused by the SEI growth.

The simulation results indicated that after a single aging process, the capacity loss errors caused by the growth of the SEI were 1.29%, 1.77%, and 1.78%, and the errors in the increase of internal resistance were 2.33%, 3.25%, and 2.26%, respectively. The simulation revealed that during the charging process, the growth rate of the SEI showed an upward trend, while during the discharging process, the growth rate of the SEI exhibited a downward trend. Additionally, when charging and discharging at the same rate, more SEI was formed during charging than during discharging. Throughout the aging cycles, the proportion of capacity loss caused by the SEI first decreased, then increased, and finally decreased again. As the aging experiments progressed, the coverage of the SEI on the electrode surface tended to become more uniform, but the unevenness in its thickness also became increasingly pronounced.

These findings offer new insights into the impact of discharge rates on the SEI growth mechanism, with the potential to apply the simulation results to actual battery design and performance assessment. They may also guide the optimization of battery operating conditions to slow down the growth rate of the SEI, thereby enhancing the performance and lifespan of the battery.

## Acknowledgments

**Funding:** This work was jointly supported by the Youth Foundation of the Natural Science Foundation of Shandong Province (grant no. ZR2023QE036).

**Author contributions:** J.L.: conceptualization, supervision, project administration, writing—review and editing (lead), and funding acquisition. X.H.: formal analysis, investigation, writing—original draft, writing—review and editing (equal), and visualization. T.L.: formal analysis and investigation.

**Competing interests:** The authors declare that they have no competing interests.

## Data Availability

Data will be made available on request.

## Supplementary Materials

Appendix A and B  
Tables S1 to S5

## References

- Colclasure AM, Li X, Cao L, Finegan DP, Yang C, Smith K. Significant life extension of lithium-ion batteries using compact metallic lithium reservoir with passive control. *Electrochim Acta*. 2021;370:Article 137777.
- Geng Z, Wang S, Lacey MJ, Brandell D, Thiringer T. Bridging physics-based and equivalent circuit models for lithium-ion batteries. *Electrochim Acta*. 2021;372:Article 137829.
- Yu Q, Wang C, Li J, Xiong R, Pecht M. Challenges and outlook for lithium-ion battery fault diagnosis methods from the laboratory to real world applications. *eTransportation*. 2023;17:Article 100254.
- Peled E, Menkin S. Review—SEI: Past, present and future. *J Electrochem Soc*. 2017;164(7):A1703–A1719.
- Sun T, Shen T, Zheng Y, Ren D, Zhu W, Li J, Wang Y, Kuang K, Rui X, Wang S, et al. Modeling the inhomogeneous lithium plating in lithium-ion batteries induced by non-uniform temperature distribution. *Electrochim Acta*. 2022;425:Article 140701.
- Li X, Zeng T, Qin H, Huo R, Liu Y, Wei D, Ding X. Investigation of inhomogeneous degradation in large-format lithium-ion batteries. *J Energy Storage*. 2021;42:Article 103113.
- Zhuo M, Offer G, Marinescu M. Degradation model of high-nickel positive electrodes: Effects of loss of active material and cyclable lithium on capacity fade. *J Power Sources*. 2023;556:Article 232461.
- Bond T, Gauthier R, Eldesoky A, Harlow J, Dahn JR. In situ imaging of electrode thickness growth and electrolyte depletion in single-crystal vs polycrystalline  $\text{LiNixMnyCozO}_2$ /graphite pouch cells using multi-scale computed tomography. *J Electrochem Soc*. 2022;169:Article 020501.
- Stockhausen R, Gehrlein L, Müller M, Bergfeldt T, Hofmann A, Müller FJ, Maibach J, Ehrenberg H, Smith A. Investigating the dominant decomposition mechanisms in lithium-ion battery cells responsible for capacity loss in different stages of electrochemical aging. *J Power Sources*. 2022;543: Article 231842.
- Agubra V, Fergus J. Lithium ion battery anode aging mechanisms. *Materials*. 2013;6(4):1310–1325.
- Börner M, Friesen A, Grützke M, Stenzel YP, Brunklaus G, Haetge J, Nowak S, Schappacher FM, Winter M. Correlation of aging and thermal stability of commercial 18650-type lithium ion batteries. *J Power Sources*. 2017;342:382–392.
- Galatro D, Silva CD, Romero DA, Trescases O, Amon CH. Challenges in data-based degradation models for lithium-ion batteries. *Int J Energy Res*. 2020;44(4):3954–3975.
- Heiskanen SK, Kim J, Lucht BL. Generation and evolution of the solid electrolyte interphase of lithium-ion batteries. *Joule*. 2019;3(10):2322–2333.
- Zhao W, Zhao C, Wu H, Li L, Zhang C. Progress, challenge and perspective of graphite-based anode materials for lithium batteries: A review. *J Energy Storage*. 2024;81: Article 110409.
- Peled E. The electrochemical behavior of alkali and alkaline earth metals in nonaqueous battery systems—The solid electrolyte interphase model. *J Electrochem Soc*. 1979;126:2047–2051.
- Aurbach D. Review of selected electrode–solution interactions which determine the performance of Li and Li ion batteries. *J Power Sources*. 2000;89:206–218.

17. Wang L, Liu T, Wu T, Lu J. Exploring new battery knowledge by advanced characterizing technologies. *Exploration*. 2021;1(3):20210130.
18. Feng G, Jia H, Shi Y, Yang X, Liang Y, Engelhard MH, Zhang Y, Yang C, Xu K, Yao Y, et al. Imaging solid–electrolyte interphase dynamics using operando reflection interference microscopy. *Nat Nanotechnol*. 2023;18(7):780–789.
19. Wang J, Yang J, Xiao Q, Zhang J, Li T, Jia L, Wang Z, Cheng S, Li L, Liu M, et al. In situ self-assembly of ordered organic/inorganic dual-layered interphase for achieving long-life dendrite-free Li metal anodes in LiFSI-based electrolyte. *Adv Funct Mater*. 2021;31(7):2007434.
20. Smith K, Shi Y, Santhanagopalan S. Degradation mechanisms and lifetime prediction for lithium-ion batteries—A control perspective. *Am Control Conf*. 2015;2015:728–730.
21. Zhuo Z, Lu P, Delacourt C, Qiao R, Xu K, Pan F, Harris SJ, Yang W. Breathing and oscillating growth of solid-electrolyte-interphase upon electrochemical cycling. *Chem Commun*. 2018;54(7):814–817.
22. Malmgren S, Ciosek K, Hahlin M, Gustafsson T, Gorgoi M, Rensmo H, Edström K. Comparing anode and cathode electrode/electrolyte interface composition and morphology using soft and hard X-ray photoelectron spectroscopy. *Electrochim Acta*. 2013;97:23–32.
23. Nie M, Chalasani D, Abraham DP, Chen Y, Bose A, Lucht BL. Lithium-ion battery graphite solid electrolyte interphase revealed by microscopy and spectroscopy. *J Phys Chem C*. 2013;117(3):1257–1267.
24. Yang X, Leng Y, Zhang G, Ge S, Wang C. Modeling of lithium plating induced aging of lithium-ion batteries: Transition from linear to nonlinear aging. *J Power Sources*. 2017;360:28–40.
25. Yang S, Hua Y, Qiao D, Lian Y, Pan Y, He Y. A coupled electrochemical-thermal-mechanical degradation modelling approach for lifetime assessment of lithium-ion batteries. *Electrochim Acta*. 2019;326:Article 134928.
26. Ramadass P, Haran B, Gomadam PM, White R, Popov BN. Development of first principles capacity fade model for Li-ion cells. *J Electrochem Soc*. 2004;151(2):A196–A203.
27. Safari M, Morcrette M, Teyssot A, Delacourt C. Multimodal physics-based aging model for life prediction of Li-ion batteries. *J Electrochem Soc*. 2009;156(3):A145–A153.
28. Wang A, Kadam S, Li H, Shi S, Qi Y. Review on modeling of the anode solid electrolyte interphase (SEI) for lithium-ion batteries. *npj Comput Mater*. 2018;4:15.
29. Liu P, Miao L, Sun Z, Chen X, Si Y, Wang Q, Jiao L. Inorganic-organic hybrid multifunctional solid electrolyte interphase layers for dendrite-free sodium metal anodes. *Angew Chem Int Ed*. 2023;62(47):Article e202312413.
30. Gao J, Wang G, Luo KH. Formation of solid electrolyte interphase in Li-ion batteries: Insights from temperature-accelerated ReaxFF molecular dynamics. *Appl Energy*. 2024;371:Article 123708.
31. Song X, Li S, Li X, Zhang Y, Wang X, Bai Z, Kheimeh Sari HM, Zhao Y, Zhang J. A lattice-matched interface between in situ /artificial SEIs inhibiting SEI decomposition for enhanced lithium storage. *J Mater Chem A*. 2020;8:11165–11176.
32. Barter D, Spotte-Smith EWC, Redkar NS, Dwaraknath S, Persson KA, Blau SM. Template-free reaction networks enable predictive and automated analysis of complex electrochemical reaction cascades. *ESC Meet Abstr*. 2022;MA2022-01:1945.
33. Wang L, Menakath A, Han F, Wang Y, Zavalij PY, Gaskell KJ, Borodin O, Iuga D, Brown SP, Wang C, et al. Identifying the components of the solid-electrolyte interphase in Li-ion batteries. *Nat Chem*. 2019;11(9):789–796.
34. Spotte-Smith EWC, Kam RL, Barter D, Xie X, Hou T, Dwaraknath S, Blau SM, Persson KA. Toward a mechanistic model of solid-electrolyte interphase formation and evolution in lithium-ion batteries. *ACS Energy Lett*. 2022;7(4):1446–1453.
35. Shinagawa C, Ushiyama H, Yamashita K. Multiscale simulations for lithium-ion batteries: SEI film growth and capacity fading. *J Electrochem Soc*. 2017;164(13):A3018–A3024.
36. Liu L, Feng X, Lu L, Han X, Ouyang M, Wu B, Lu W. Kinetic Monte Carlo simulation of lithium dendrite growth in lithium-ion battery. Paper presented at: 2021 IEEE 4th International Electrical and Energy Conference (CIEEC); 2021 May 29–30; Wuhan, China.
37. Li J, Wang D, Deng L, Cui Z, Lyu C, Wang L, Pecht M. Aging modes analysis and physical parameter identification based on a simplified electrochemical model for lithium-ion batteries. *J Energy Storage*. 2020;31:Article 101538.
38. Luo W, Lyu C, Wang L, Zhang Q. A new extension of physics-based single particle model for higher charge–discharge rates. *J Power Sources*. 2013;241:295–310.
39. Ning G, Popov BN. Cycle life modeling of lithium-ion batteries. *J Electrochem Soc*. 2004;151(10):A1584–A1591.
40. Idemoto Y, Richardson JW Jr, Koura N, Kohara S, Loong C. Crystal structure of  $(\text{Li}_{x}\text{K}_{1-x})_{2}\text{Co}_3$  ( $X = 0, 0.43, 0.5, 0.62, 1$ ) by neutron powder diffraction analysis. *J Phys Chem Solids*. 1998;59(3):363–376.
41. Zhang D, Haran BS, Durairajan A, White RE, Podrazhansky Y, Popov BN. Studies on capacity fade of lithium-ion batteries. *J Power Sources*. 2000;91:122–129.